Biosensors and Bioelectronics 180 (2021) 113117

Contents lists available at ScienceDirect

Biosensors and Bioelectronics

journal homepage: http://www.elsevier.com/locate/bios

Short communication

Site-specifically wired and oriented glucose dehydrogenase fused to a minimal cytochrome with high glucose sensing sensitivity

Itay Algov, Aviv Feiertag, Lital Alfonta *

Departments of Life Sciences, Chemistry and Ilse Katz institute for Nanoscale Science and Technology, Ben-Gurion University of the Negev, PoBox 653, Beer-Sheva, 8410501, Israel

ARTICLE INFO

Keywords:
Direct electron transfer (DET)
Glucose biosensor
Glucose dehydrogenase (GDH)
Site-specific wiring
Unnatural amino acids
Click chemistry

ABSTRACT

Direct electron transfer based enzymatic biosensors are highly efficient systems where electrons are transferred directly from the enzyme's electroactive site to the electrode. One way of achieving it is by 'wiring' the enzyme to the electrode surface. The wiring of enzymes to electrode surfaces can be reached in many different ways but controlling its orientation towards the electrode surface is still a challenge. In this study we have designed a Flavin-adenine dinucleotide dependent glucose dehydrogenase that is fused to a minimal cytochrome with a site-specifically incorporated unnatural amino acid to control its orientation towards the electrode. Several site-specifically wired mutant enzymes were compared to each other and to a non-specifically wired enzyme using atomic force microscopy and electrochemical techniques. The surface and activity analyses suggest that the site-specific wiring through different sites maintains the correct folding of the enzyme and have a positive effect on the apparent electrochemical electron transfer rate constant k_{ET}^{app}. Electrochemical analysis revealed an efficient electron transfer rate with more than 15 times higher i_{max} and 10-fold higher sensitivity of the site-specifically wired enzyme variants compared to the non-specifically wired ones. This approach can be utilized to control the orientation of other redox enzymes on electrodes to allow a significant improvement of their electron transfer communication with electrodes.

1. Introduction

Electrochemical enzymatic biosensors are widely used for the detection of different metabolites such as glucose (Algov et al., 2017), cholesterol (Huang et al., 2018), alcohol (Mohan et al., 2017), lactate (Calabria et al., 2017), ammonia (Sasaki et al., 2018) and many more. Analytes can be reduced or oxidized by an enzyme while currents can be produced and correlated to analyte concentration. Electron transfer (ET) between the enzyme active-site to an electrode can be mediated using an electrochemical mediator molecule (Bingham et al., 2020; Vilian et al., 2019; Wang et al., 2019) or directly to the electrode (Bollella and Katz, 2020; Ito et al., 2019; López Marzo et al., 2020). Direct electron transfer (DET) type biosensors allow high efficiency and low costs while mediated electron transfer (MET) based biosensors are often limited by diffusion and require the addition of external molecules that are expensive and at times toxic. Hence, DET type biosensors are highly desirable (Habermüller et al., 2000). The use of enzymes allows the detection of many different molecules with high specificity, selectivity and sensitivity. On the other hand, proteins are insulating molecules, their activity is dependent on different conditions such as pH and temperature, their catalytic activity decreases overtime due to misfolding or aggregation and substrate accessibility to the enzyme active-site is sometimes deterred due to enzyme orientation on the electrode surface (Bollella and Gorton, 2018; Bollella and Katz, 2020; Okuda-Shimazaki et al., 2020).

In order to allow DET, several different wiring approaches were taken for protein immobilization onto electrode surfaces. One efficient wiring approach is the use of redox active polymers, which requires the use of modified polymers, to encapsulate the enzyme, allowing proximity to the active-site and ET through active redox centers (Heller, 1990; Marquitan et al., 2020; Yuan and Minteer, 2019). Another approach is the use of semi-conductive hydro-gels such as reduced graphene oxide to entrap the protein and allow access to its redox active co-factor (Palanisamy et al., 2019; Ravenna et al., 2015; Zhou et al., 2019). The use of such materials allows encapsulation of the enzyme which gives it stability, however, without the ability to control its orientation. To overcome that, it is possible to wire the enzyme directly to an electrode.

* Corresponding author.
E-mail address: alfontal@bgu.ac.il (L. Alfonta).

https://doi.org/10.1016/j.bios.2021.113117
Received 17 December 2020; Received in revised form 22 February 2021; Accepted 23 February 2021
Available online 27 February 2021

With the emergence of more wearable biosensing devices (Alfonta, 2021; Min et al., 2021; Sempionatto et al., 2021), the need for non-invasive biosensing devices increases. However, sensing of bodily fluids such as sweat, tears and urine requires much more sensitive devices then those designed for blood metabolites and biomarkers sensing (Strakosas et al., 2019). In order to achieve such sensitivity, direct wiring and orientation of enzymes is needed. Direct and site-specific wiring of enzymes can be achieved by using chemical modifications such as exploiting thiol-gold chemistry with gold electrodes via protein's surface exposed cysteins or deletion mutations that result in a single cysteine residue (Holland et al., 2011). N-Ethyl--N′-(3-dimethylaminopropyl)carbodiimide (EDC) coupling through lysine or carboxylic residues of native amino acids (Lopez et al., 2015; Willner and Katz, 2000), biological modifications through fusion of gold-binding peptides (Lee et al., 2020) or carbon nano tubes (CNT) binding peptides (Wang et al., 2003) to the N- or C- termini of the target enzyme. The use of native amino acids such as lysines for EDC coupling or cysteines for thiol-gold chemistry requires highly purified samples and can result in undesirable binding of misfolded proteins, which may expose core residues, resulting in an insulating film on the electrode surface. Moreover, the use or the deletion of surface exposed lysines or cysteins often critically affects protein folding and eliminating them may lead to misfolding of the protein of interest. Using gold or CNT binding peptides is restricted to the N- or C- termini of the protein sequence, hence limited to one or two possible orientations of the redox enzyme towards the electrode. The use of a biorthogonal chemical handle in a pre-selected site that could be in a non-structured domain of the enzyme, may help with the above-mentioned limitations.

The use of unnatural amino acids (UAAs) with a designated residue that allows biorthogonal chemical modification which can be encoded in any given site of the protein, resulting in a precise and controlled site-specific wiring of the protein to an electrode (Amir et al., 2013; Schlesinger et al., 2018; Xia et al., 2019). The use of a UAA can provide a unique functional group that allows enzyme orientation towards the electrode, which is a key factor on the way to efficient DET. In this study, we have used the UAA Propargyl-l-lysine (PrK) (Fig. 1B (**1**)) to site-specifically wire Flavin-adenine dinucleotide glucose dehydrogenase (FAD-GDH) fused to a minimal cytochrome c domain (MCD) (FGM) mutants (Fig. 1A) (Algov et al., 2017) as well as Flavin-adenine dinucleotide glucose dehydrogenase (GDH), through Copper(I)-catalysed azide-alkyne cycloaddition (click) reaction to an azide-pyrene (Fig. 1B (**2**)), to a glassy-carbon electrode (GCE) and compared its immobilization on the electrode surface and its electrochemical performance to a non-specifically wired FGM using EDC coupling to a pyrene-carboxylic acid linker (PCA) (Fig. 1B (**3**)). Atomic force microscopy (AFM) revealed that the site-specifically wired enzyme showed a scattered surface coverage and electrochemical measurements revealed ca. 10 times higher catalytic currents compared to the non-specifically wired FGM with higher ET rates. We have also found that site-specific wiring of the enzymes through different sites affect the k_{ET}^{app} value. In addition, the combination of AFM and cyclic voltammetry (CV) measurements have

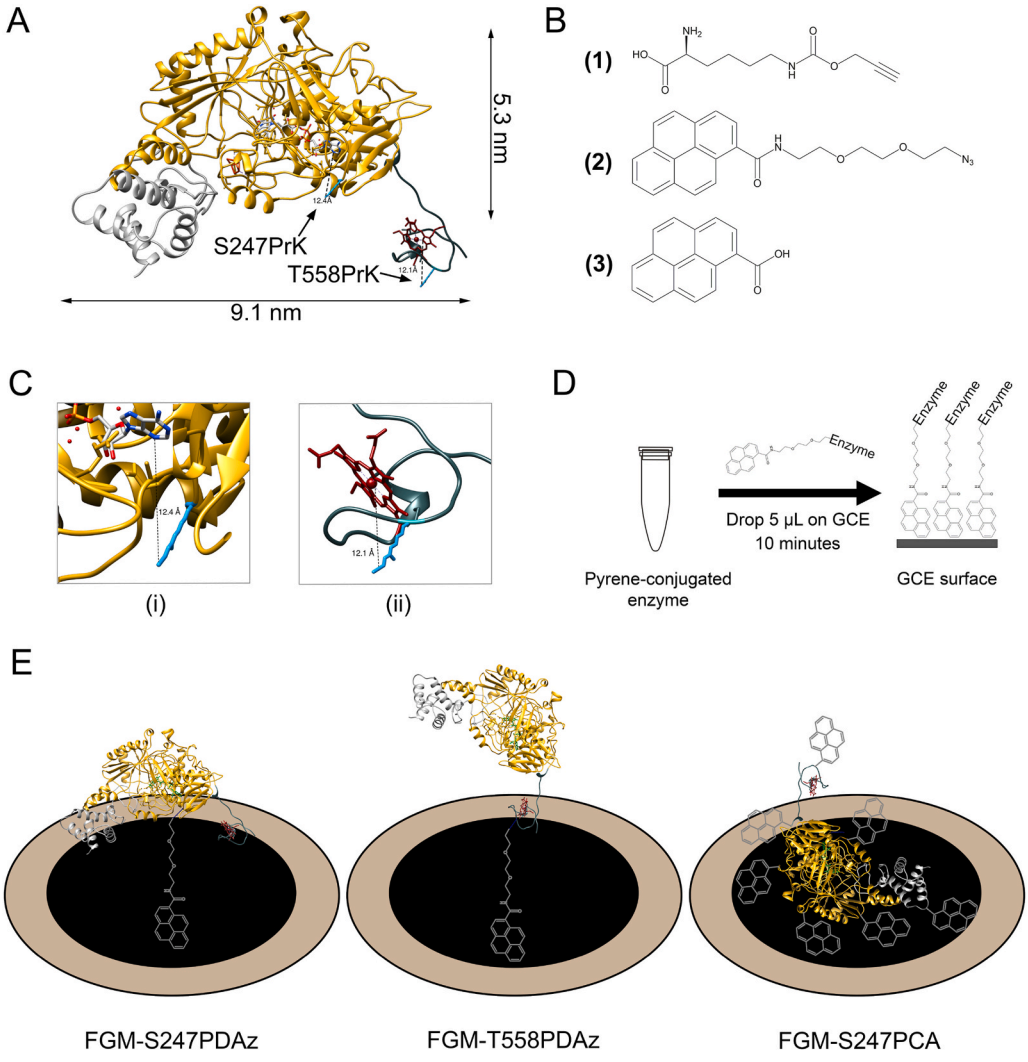

Fig. 1. FGM structural model **A.** The structure of FGM was modeled by fusing the crystal structure of FAD-GDH from *burkholderia cepacia* (γ-subunit in silver, α-subunit in gold, PDB ID: 6A2U) to the crystal structure of MCR2 domain from MamP crystal structure in dark green (PDB ID: 4JJ0). Dimensions of protein's height and width were estimated using UCSF chimera software (Pettersen et al., 2004). PrK at positions S247 and T558 are labeled in light blue, FAD co-factor is blue, heme is dark red. **B.** Chemical structures of PrK (**1**), pyrene-diethyleneglycol-azide (PDAz) (**2**) and PCA (**3**). **C.** Distance measurements between S247PrK residue and the FAD co-factor (i) and between the T558PrK residue and the heme domain (ii). **D.** Schematic illustration of the glassy-carbon electrode modification procedure **E.** Schematic illustration of the expected orientation of FGM-S247PDAz, FGM-T558PDAz and FGM-S247PCA on the electrode surface. (For interpretation of the references to color in this figure legend, the reader is referred to the Web version of this article.)

revealed, that while site-specific wiring through a single-site of attachment retained enzyme fold and activity, the non-specifically attached enzyme through EDC coupling has aggregated and mostly lost its native structure and activity.

2. Experimental section

2.1. UAA incorporation into FGM

Escherichia coli(E. coli) BL21 bacterial expression system was used for the expression of the FGM enzyme with site-specifically incorporated UAA. Pyrrolysyl orthogonal translation system (pylOTS) DNA sequence was amplified from the pEVOL plasmid using polymerase chain reaction (PCR) and cloned into the backbone of pec86 plasmid using Gibson's assembly to generate a new plasmid called pec86-pylOTS (Fig. S4A). pylOTS allows the continuous expression of an orthogonal translation system (orthogonal tRNA and aminoacyl tRNA synthetase) for incorporation of PrK (**1**) using the amber (TAG) stop codon suppression (Chemla et al., 2018), while the pec86 plasmid is responsible for the continuous expression of *E. coli* cytochrome c maturation system (Arslan et al., 1998). The second plasmid, pETDuet-FGM (Fig. S4B) was used for the expression of FGM with a TAG mutation encoded in the desired incorporation site. Four different TAG mutants were prepared using site-directed mutagenesis, according to GDH crystal structure. Our guiding rational for mutation sites was to control the enzyme orientation in a manner that will allow proximity of 14 Å or less between the FAD or heme site and the electrode, without interference with the protein structure and correct folding. The sites that were tested were R42TAG and S247TAG, which are in close proximity to the FAD binding-site, while T558TAG (Fig. 1Cii) is in a close proximity to the heme domain. For the FAD proximity mutation site, we had the highest expression levels and activity with the S247TAG mutant (Fig. 1Ci). Hence, from here on we have focused our studies on S247TAG and T558TAG mutants. As a control that will allow us to find out whether the MCD affects ET properties of a site-specifically wired enzyme, we have also generated an S247TAG mutant GDH that lacks its MCD domain.

2.2. Protein conjugation with pyrene containing linkers

For the site-specific wiring of FGM-S247PrK, FGM-T558PrK and GDH-S247PrK we have used a pyrene-diethyleneglycol-azide (PDAz) linker (**2**). The azide in (**2**) was clicked to the alkyne residue of (**1**). 3 μM of protein sample was mixed with 400 μM (**2**), 2 mM tris pH = 8.2, 10 mM KCl, 1 mM Cu(I), 1.2 mM THPTA, 2.5 mM Sodium L-ascorbate (NaAsc) and 10% Dimethyl sulfoxide (DMSO). The reaction was incubated for 1 h in the dark at room temperature with shaking, then transferred to 4 °C for two days before use. For the non-specific wiring of FGM-S247PrK we have used a standard EDC-N-Hydroxysuccinimide (NHS) coupling with a PCA linker (**3**). 3 μM of protein sample was mixed with 200 mM EDC, 400 mM NHS, 25 mM 4-(2-hydroxyethyl)-1-piperazineethanesulfonic acid (HEPES) buffer pH = 7.0 and 100 μM (**3**) and incubated for 12 h at RT with shaking.

2.3. Electrode preparations and electrochemical measurements

Glassy carbon electrode was first polished on 0.05 μm alumina polishing pad followed by five minutes sonication in DDW and drying using pure argon gas. Protein wiring to electrode was performed by dropping 5 μL of 3 μM pyrene-conjugated protein sample on GCE surface for 10 minutes incubation at RT (Fig. 1D) to allow the wiring of the protein through pi-pi stacking interactions between the pyrene groups and the GCE surface (Milton et al., 2016; Stergiou et al., 2020). After 10 minutes, the electrode was rinsed with DDW to remove unbound molecules and measured using a standard 3-electrodes electrochemical system with Ag/AgCl reference electrode and a pencil rod as the counter electrode. The expected orientations of all FGM variants towards the electrode are presented in Fig. 1E. GDH-S247PDAz is not presented since it is expected to be oriented like FGM-S247PDAz, lacking MCD. All measurements were performed using Palmsense 3 potentiostat (Palm Instruments, Houten, The Netherlands) at RT in 100 mM acetate buffer pH = 5.0 under argon atmosphere and at variable scan rates. DPV measurements were performed with potential pulse of 100 mV for 0.1 sec, with scan rate of 25 mV/sec. In the multistep amperometry measurements the electrode's potential was biased from (-200) mV to 0 mV, framing the onset potentials of all modified electrodes, measuring the current decay for 10 sec for each step. In case of negative current values, a constant value was added to allow current decay linearization using natural logarithm (ln) transformation. To test the enzyme-electrode performance in the presence of interfering molecules, we have used acetate buffer supplemented with 50 μM ascorbic acid, 10 mM lactate and 10 mM urea (ALU) and measured the current response upon application of 150 mV vs. Ag/AgCl reference electrode.

3. Results and discussion

3.1. Enzyme characterization

FGM-S247PrK expression was first verified using anti His-tag Western-blot analysis (Fig. S1A). Two expression cultures were grown, while only one of them was supplemented with 2 mM of (**1**), the cells were then lysed and analyzed. It can be seen that only with the supplementation of (**1**) to the expression culture we could observe a 67 kDa band indicating the successful expression of a full-length His-tagged protein. In the absence of (**1**) in the growth culture, we could not detect any protein band in the relevant size. The incorporation of (**1**) into the protein was verified by "clicking" a tetramethylrhodamine-Azide (TAMRA-Az) to the FGM-S247PrK, GDH-S247PrK and FGM-T558PrK protein variants. Fluorescent gel image (Fig. S2) has demonstrated that the mutants of FGM and GDH indeed had (**1**) incorporated into their amino-acid sequence. One band in the expected size indicated that the FGM/GDH mutants are the only proteins in the sample that contain the alkyne residue of (**1**). Next, we have used in-gel heme staining to verify a proper minimal cytochrome c maturation process (Fig. S1B), where a band of around 67 kDa was observed, indicating a successful heme maturation. The enzyme's catalytic activity towards glucose was tested biochemically using 2,6-Dichlorophenolindophenol (DCIP) colorimetric assay for glucose oxidation (Fig. S1C). The colorimetric activity assay indicated that FGM-S247PrK, GDH-S247PrK and FGM-T558PrK are all capable of oxidizing glucose with a similar specific activity (data not shown).

3.2. AFM measurements

Understanding protein orientation on carbon surface can be realized by the combination of the knowledge we have from the protein crystal structure (Fig. 1A) with AFM measurements. We have analyzed the topography of an atomically flat carbon surface after wiring FGM-S247 using different methods and compared it to the known expected size of the protein. Fig. S6 shows the AFM measurements of HOPG surfaces after 10 minutes of incubation in acetate buffer (i), FGM-S247 wired through (**2**) (ii) and FGM-S247 wired through (**3**) (iii). Since HOPG is atomically flat, we could measure the height of the bound enzyme on the HOPG surface and compare it to an approximate enzyme foot-print and height calculated from the crystal structure of FAD-GDH (Fig. 1A) taking into account the estimated lengths of the respective linkers. As a control, acetate buffer added to the surface, did not result in salt accumulation (Fig. S6(i)). Measurement of the FGM-S247 linked through (**3**) showed islands of bound molecules averaging around 70 nm in height, almost 10 times higher than the height expected from a monolayer of FGM. These islands may be a result of protein aggregation caused by the wiring of the enzyme through multiple sites through non-specific wiring. Coupling to (**3**) may result in multiple pyrene molecules on each protein. The

adhesion of the protein to the surface through multiple pyrene residues can expose the hydrophobic core of the protein, which may result in the aggregation observed in the AFM measurements. However, measurement of the FGM-S247 clicked to (**2**) showed scattered particles on the surface with an average height of ca. 6 nm. When taking into consideration the anchoring point of the protein (S247) and the length of (**2**) (which is estimated to be 0.6 nm in its stretched form), this observation is very close to the estimated height of a single layer of a wired FGM in its expected orientation (Fig. 1A) on the HOPG surface. These results suggest that using site-specific wiring affords a relatively good control over the protein orientation towards the surface as well as better surface coverage of active and correctly folded enzyme with a mono-layer pattern, although not a densely packed one, rather than multi layered and partially unfolded aggregates.

3.3. Electrochemical characterization

For the electrochemical characterization of the wired enzyme, three different enzyme variants were compared using a site-specific wiring approach with the PDAz linker. In addition, the site-specific wiring approach was compared to a non-specific wiring approach using EDC-NHS coupling of one of the mutants to the electrode (FGM-S247PCA). In order to see whether we can detect the electroactive peaks and differentiate between the wiring approaches we have conducted DPV measurements that are more sensitive and less prone to background from non-Faradaic currents. Fig. 2A shows DPVs of FGM-S247PDAz and FGM-S247PCA in the absence of glucose. While FGM-S247PCA shows two well-defined peaks at (-100) mV and (+75) mV, FGM-S247PDAz shows a minute peak at (-250) mV and a defined albeit wide peak at ca. 0 mV vs. Ag/AgCl reference electrode. A control experiment where the DPV was performed on the conjugation reagents only (without adding protein samples) shows that the observed peaks indeed originate from FGM electroactive-sites (Fig. S7) and not from the presence of other factors in the reaction mixture.

In order to elucidate the source of the two defined peaks in the non-specifically bound enzyme compared with the broad peak in the site-

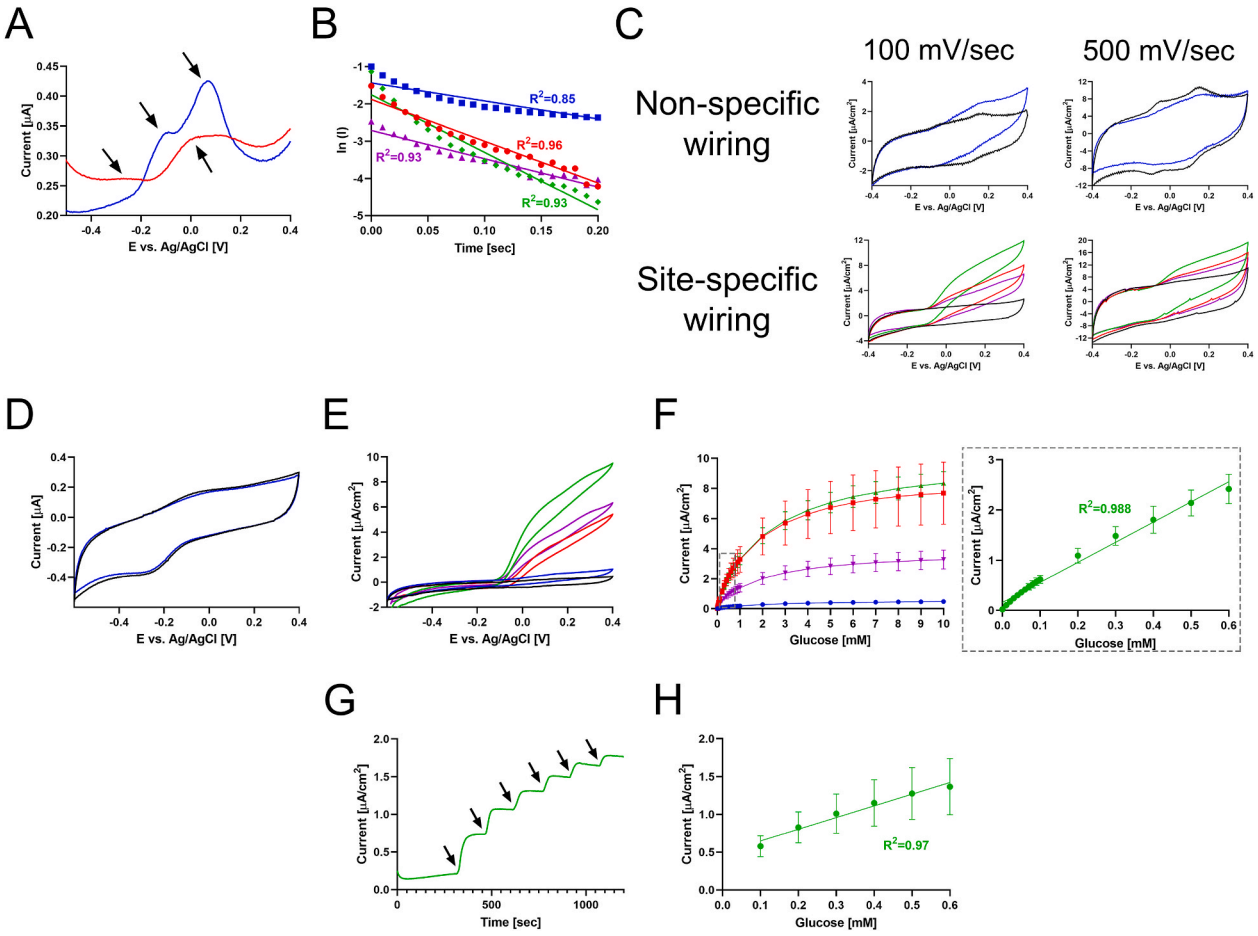

Fig. 2. Electrochemical characterization of wired FGM and GDH. **A.** DPV measurements of FGM-S247PDAz (red) and FGM-S247PCA (blue) under argon in the absence of glucose. Peaks are indicated by black arrows. **B.** Linearized multistep amperometry current decay plot of FGM-S247PDAz (red), FGM-T558PDAz (green), GDH-S247PDAz (purple) and FGM-S247PCA (blue). **C.** CVs of FGM-S247PDAz, FGM-T558PDAz, GDH-S247PDAz and FGM-S247PCA in high scan rates before (black) and after (red, green, purple and blue, respectively) the addition of 5 mM glucose. **D.** CV of heme-binding domain attached to the electrode surface before (black) and after (blue) the addition of 5 mM of glucose. **E.** CVs in scan rate of 10 mV/sec for FGM-S247PDAz, FGM-T558PDAz, GDH-S247PDAz and FGM-S247PCA before (black) and after (red, green, purple and blue, respectively) the addition of 5 mM glucose (scan rate 10 mV/sec). **F.** Glucose-current calibration curves of FGM-S247PCA (blue), FGM-S247PDAz (red), FGM-T558PDAz (green) and GDH-S247PDAz (purple) measured using chronoamperometric detection upon application of 300 mV vs. Ag/AgCl reference electrode. The current from each glucose concentration (10 µM - 10 mM) was measured in triplicates; curves of the mean currents are presented with standard deviations. Inset presents the current response of FGM-T558PDAz towards glucose in physiologically relevant glucose concentrations of sweat and tears. **G.** FGM-T558PDAz response to glucose in ALU interference solution that was measured upon application of 150 mV vs. Ag/AgCl reference electrode. Black arrows indicate 0.1 mM glucose additions. **H.** The current response of FGM-T558PDAz in physiologically relevant range of glucose in the presence of interfering molecules. The current was measured in triplicates and the mean current values were used for the linear regression and are presented with error bars. (For interpretation of the references to color in this figure legend, the reader is referred to the Web version of this article.)

specifically bound enzyme, we have calculated the apparent ET coefficient (k_{ET}^{app}) using multistep amperometry as was previously described by us (Schlesinger et al., 2018). In Fig. 2B it can be seen that the linearized current decay of the site-specifically wired enzyme has a mono-exponential decay characteristic (R^2>0.93) while the non-specifically wired enzyme has a bi-exponential decay dependence, which indicates ET from one or two redox-active sites. It cannot be excluded that the observed mono-exponential characteristic signal is an average from both, FAD and heme domain, but it can be deduced from this result that only one orientation is dominant on the electrode surface. Hence, we could extract k_{ET}^{app} values from the slope of the linearized current decay curve as summarized in Table 1. Since we have observed a mono-exponential current decay from the site-specifically bound enzymes variants and a bi-exponential current decay from the non-specifically bound one, it could be an indication of the source of the two peaks: whereas one peak origin is a direct communication between the heme and the electrode and the other is a mediated ET from the FAD to the heme and then to the electrode. We hypothesize that the porphyrin, in the case of non-specific attachment is adsorbed directly on the electrode due to two lysine residues in a close proximity to its binding-site. Whereas an internal ET (between the FAD and the heme) can be hardly observed when fast scan rates are being used as no electrocatalytic current is apparent in the presence of glucose under higher scan rates regime and only the two separate peaks are visible and are well defined (which is an indication of Faradaic processes but not catalytic ones) (Fig. 2C). This result is in agreement with a control experiment that have shown that no electrocatalytic current is observed from attaching the heme binding domain only to the electrode in the presence of glucose as it cannot oxidize glucose in the absence of the FAD binding domain (Fig. 2D).

Fig. 2E shows the bioelectrocatalytic currents of three site-specifically wired variants and one non-specifically wired enzyme in response to 5 mM glucose addition using CV with a slow potential scan rate of 10 mV/sec. As oppose to high-potential-scan rate measurements (Fig. 2C), at a low scan rate, we can observe the catalytic currents from the different variants almost independently from ET rates (provided that those ET rates are faster than the potential scan rate). The catalytic response of the site-specifically wired enzymes is much higher compared to the non-specifically wired enzyme (ca. 10 folds higher increase in maximal currents) and its onset potential is lower (-100 mV for all the site-specifically wired enzymes compared to -45 mV for FGM-S247PCA). This result indicates better accessibility of the protein's electroactive site towards the electrode. Within the site-specifically wired enzymes, both GDH-S247PDAz and FGM-S247PDAz, which are bound with proximity to the FAD domain, present almost the same catalytic current while the FGM-T558PDAz shows almost two-fold higher catalytic current compared to both of them. In the site-specifically wired enzyme the substrate has a direct access to the catalytic site and the electrons can be transferred directly to the electrode without any barriers. By comparing the two points of attachment, it was evident that higher catalytic currents are observed when the enzyme was wired close to its cytochrome domain (FGMT558TAG) rather than through sites that are close to its FAD binding-site (FGMS274TAG). While with the non-specifically wired enzyme, ET can be deterred by proteins covering the electrode in different orientations that are not optimal for efficient ET.

For a given glucose concentration, the highest catalytic current was observed for FGM-T558PDAz variant, followed by FGM-S247PDAz and the lower catalytic current was observed with the GDH-S247PDAz electrode. Using high potential scan rates can help us understand whether the MCD has a role in the electron transfer to the electrode. While using low potential-scan rates resulted in almost the same catalytic current for both GDH and FGM, which are wired through the S247 site, using high scan rates resulted in higher currents for FGM. This observation suggests that the MCD participates in the ET process to the electrode, rendering it more efficient.

Apparent electron transfer rate constants were determined for the different variants. The highest k_{ET}^{app} was observed for FGM-T558PDAz wired to the electrode close to its MCD, next was the FGM-S247PDAz wired close to its FAD binding-site, a lower value was that of GDH-S247PDAz which is wired in a close proximity to its FAD however, in the absence of MCD and the lowest value was that of the non-specifically wired FGM-S247PCA. Glucose concentration vs. current calibration curves of all variants are presented in Fig. 2F. It can be seen that the site-specifically wired enzymes show much higher currents than the non-specific wired ones. The apparent electrochemical Michaelis-Menten constants were determined based on a non-linear fit of the calibration curves shown in Fig. 2F (Table 1). K_M^{app} of all samples did not differ significantly between variants within the error of the measurements in the range of 1.55-1.89 mM which is an indication that the mutagenesis and the site of UAA incorporation did not modify the enzyme affinity to glucose. However, i_{max} values were calculated to be more than 15 times higher for FGM-S247PDAz with 8.88 ± 0.40 μA cm^{-2} vs. 0.55 ± 0.02 μA cm^{-2} for FGM-S247PCA. The site of attachment has also an effect on the i_{max} values. Wiring through the T558TAG site with a proximity to the heme domain resulted in the highest current value, a slightly lower value was that of the S247TAG variant and the lowest value was that of the GDH-S247TAG. This result is another indication that the MCD has an effect on the ET abilities of the protein and are in correlation with the calculated k_{ET}^{app} values. In comparison with our previously reported i_{max} value for non-wired FGM (Algov et al., 2017) which was 2.0 ± 0.5 μA cm^{-2}, the site-specific wiring demonstrates more than four times higher i_{max} value which is a significant improvement. Those high currents allow much higher resolution for glucose biosensing with higher sensitivity, which could be very useful and physiologically relevant for samples with low glucose concentrations such as sweat, subcutaneous plasma or tears samples (Iguchi et al., 2007; Li et al., 2016; Zhao et al., 2019). The limit of detection (LOD) was found to be 10 μM glucose for the site-specifically wired enzymes compared to 100 μM for the non-specifically wired enzyme, with a signal to noise ratio that is larger than 3. Since FGM-T558PDAz showed the highest currents in response to glucose, we have presented its current response to the physiologically relevant concentrations in tears and sweat in the inset of Fig. 2F. FGM-T558PDAz presents a resolution of 10 μM glucose and high linearity (R^2 = 0.988) of the current measured in the 0.01 to 0.6 μM of glucose concentrations regime. The broader linear range of FGM-T558PDAz was found to be 0.01–2 mM glucose while FGM-S247PCA showed a linear range of 0.1–2 mM only (both with R^2 > 0.92) (Fig. S5). Improving the surface coverage will allow more available reaction sites (in a similar manner as improving enzyme specific activity, this could be achieved by using porous electrodes for example) that can result in a broader dynamic range. To test our wired enzyme response in the presence of interfering molecules, we have used known interfering molecules in tears samples as previously described (Yao et al., 2011). The current response of FGM-T558PDAz was tested in ALU solution upon the addition of 0.1 mM glucose increments (Fig. 2G). The current response in the physiologically relevant glucose concentrations in tears (0.1-0.6 mM) was found linear under these conditions as shown in Fig. 2H, no interference was observed under these conditions. Being able to detect glucose in the relevant concentrations without being interfered by the ALU solution makes our system suitable for glucose detection in bodily fluids other than blood.

Table 1
Apparent electrochemical constants of the different tested variants.

Enzyme variant	K_M^{app} (mM)	i_{max} (μA cm^{-2})	k_{ET}^{app} (s^{-1})
GDH-S247PDAz	1.55 ± 0.16	3.74 ± 0.12	8.0 ± 0.6
FGM-S247PDAz	1.90 ± 0.10	8.88 ± 0.40	11.2 ± 0.7
FGM-T558PDAz	1.60 ± 0.20	9.80 ± 0.20	13.4 ± 1.4
FGM-S247PCA	1.80 ± 0.20	0.55 ± 0.02	4.80 ± 0.02

4. Conclusion

In conclusion, we have presented the importance of a redox enzyme orientation towards an electrode. Non-specific wiring methods such as EDC-NHS coupling allows the covering of GCE with proteins but without the ability to control their orientation. By using site-specific UAA incorporation, we have created a unique orthogonal "chemical handle" that allows the conjugation of a linker in only one anchoring point in the protein sequence, and by that allowed determination of a specific orientation towards the electrode. The controlled orientation results in ca. 20 times higher catalytic currents in response to glucose, higher ET efficiency that was shown by the ability of the enzyme to transfer electrons in a scan rate as high as 500 mV/sec and a scattered monolayer pattern on the surface as observed by AFM measurements. Wiring of proteins through different sites result in a significant effect on their ET characteristics and their ability to communicate with an electrode. Using this method allows high flexibility in the UAA incorporation site which makes it a powerful tool for advanced protein engineering for enzyme-based biosensors. When site-specifically orienting a glucose oxidizing enzyme on the surface of an electrode, we could observe a gain in sensitivity (down to a concentration of 10 μM glucose), however, this gain in sensitivity comes with a cost, in gaining sensitivity we have lost the dynamic range that allows for higher glucose concentrations sensing. Testing FGM enzyme-electrode in ALU solution demonstrated no interference when using known interfering molecules present in tears. This makes the enzyme more suitable for non-invasive biosensors for bodily fluids other than blood such as sweat, tears and urine.

CRediT authorship contribution statement

Itay Algov: Conceptualization, Experimentation, Methodology, Investigation, Formal analysis, Writing – original draft, Writing – review & editing. **Aviv Feiertag:** experiments, Methodology, Formal analysis. **Lital Alfonta:** Conceptualization, Supervision, Project administration, Writing – review & editing.

Declaration of competing interest

The authors declare that a patent application containing information from this paper has been submitted.

Acknowledgements

This research was funded by the Israel Ministry of Science and Technology-Nanoelectronics program, grant number: 971581 and by an ISF-NSFC (Israel-China joint grant) number 2920/19. A Biotech doctoral fellowship by the Kreitman School for Graduate students at the Ben-Gurion University of the Negev is thankfully acknowledged (I.A.). We gratefully acknowledge the help of Dr. Jurgen Jopp from the Ilse Katz Institute for Nanoscale Science and Technology with the AFM measurements. Molecular graphics and analyses performed using UCSF Chimera, developed by the Resource for Biocomputing, Visualization, and Informatics at the University of California, San Francisco, with support from NIH P41-GM103311.

Appendix A. Supplementary data

Supplementary data to this article can be found online at https://doi.org/10.1016/j.bios.2021.113117.

References

Alfonta, L., 2021. Bioelectrochemistry and the singularity point "I robot"?**. Isr. J. Chem. 61, 1–9. https://doi.org/10.1002/ijch.202000113.

Algov, I., Grushka, J., Zarivach, R., Alfonta, L., 2017. Highly efficient flavin-adenine dinucleotide glucose dehydrogenase fused to a minimal cytochrome C domain. J. Am. Chem. Soc. 139, 17217–17220. https://doi.org/10.1021/jacs.7b07011.

Amir, L., Carnally, S.A., Rayo, J., Rosenne, S., Melamed Yerushalmi, S., Schlesinger, O., Meijler, M.M., Alfonta, L., 2013. Surface display of a redox enzyme and its site-specific wiring to gold electrodes. J. Am. Chem. Soc. 135, 70–73. https://doi.org/10.1021/ja310556n.

Arslan, E., Schulz, H., Zufferey, R., Künzler, P., Thöny-Meyer, L., 1998. Overproduction of the Bradyrhizobium japonicum c-type cytochrome subunits of the cbb3 oxidase in Escherichia coli. Biochem. Biophys. Res. Commun. 251, 744–747. https://doi.org/10.1006/bbrc.1998.9549.

Bingham, H., Oliveira, D., Larimer, C., Hedworth, H., Bahari, M., Watt, G.D., Harb, J.N., Lewis, R.S., 2020. Electron-mediated carbohydrate fuel cells: characterizing the homogeneous viologen-mediated electron transfer rate of carbohydrate oxidation. Renew. Energy 145. https://doi.org/10.1016/j.renene.2019.07.079, 1985–1991.

Bollella, P., Gorton, L., 2018. Enzyme based amperometric biosensors. Curr. Opin. Electrochem. 10, 157–173. https://doi.org/10.1016/j.coelec.2018.06.003.

Bollella, P., Katz, E., 2020. Enzyme-based biosensors: tackling electron transfer issues. Sensors 20, 1–32. https://doi.org/10.3390/s20123517.

Calabria, D., Caliceti, C., Zangheri, M., Mirasoli, M., Simoni, P., Roda, A., 2017. Smartphone–based enzymatic biosensor for oral fluid L-lactate detection in one minute using confined multilayer paper reflectometry. Biosens. Bioelectron. 94, 124–130. https://doi.org/10.1016/j.bios.2017.02.053.

Chemla, Y., Ozer, E., Algov, I., Alfonta, L., 2018. Context effects of genetic code expansion by stop codon suppression. Curr. Opin. Chem. Biol. 46, 146–155. https://doi.org/10.1016/j.cbpa.2018.07.012.

Habermüller, K., Mosbach, M., Schuhmann, W., 2000. Electron-transfer mechanisms in amperometric biosensors. Fresenius' J. Anal. Chem. 366, 560–568. https://doi.org/10.1007/s002160051551.

Heller, A., 1990. Electrical wiring of redox enzymes. Acc. Chem. Res. 23, 128–134. https://doi.org/10.1021/ar00173a002.

Holland, J.T., Lau, C., Brozik, S., Atanassov, P., Banta, S., 2011. Engineering of glucose oxidase for direct electron transfer via site-specific gold nanoparticle conjugation. J. Am. Chem. Soc. 133, 19262–19265. https://doi.org/10.1021/ja2071237.

Huang, Y., Tan, J., Cui, L., Zhou, Z., Zhou, S., Zhang, Z., Zheng, R., Xue, Y., Zhang, M., Li, S., Zhu, N., Liang, J., Li, G., Zhong, L., Zhao, Y., 2018. Graphene and Au NPs co-mediated enzymatic silver deposition for the ultrasensitive electrochemical detection of cholesterol. Biosens. Bioelectron. 102, 560–567. https://doi.org/10.1016/j.bios.2017.11.037.

Iguchi, S., Kudo, H., Saito, T., Ogawa, M., Saito, H., Otsuka, K., Funakubo, A., Mitsubayashi, K., 2007. A flexible and wearable biosensor for tear glucose measurement. Biomed. Microdevices 9, 603–609. https://doi.org/10.1007/s10544-007-9073-3.

Ito, Y., Okuda-Shimazaki, J., Tsugawa, W., Loew, N., Shitanda, I., Lin, C.E., La Belle, J., Sode, K., 2019. Third generation impedimetric sensor employing direct electron transfer type glucose dehydrogenase. Biosens. Bioelectron. 129, 189–197. https://doi.org/10.1016/j.bios.2019.01.018.

Lee, H., Lee, Y.S., Reginald, S.S., Baek, S., Lee, E.M., Choi, I.-G., Chang, I.S., 2020. Biosensing and electrochemical properties of flavin adenine dinucleotide (FAD)-Dependent glucose dehydrogenase (GDH) fused to a gold binding peptide. Biosens. Bioelectron. 165, 112427. https://doi.org/10.1016/j.bios.2020.112427.

Li, J., Koinkar, P., Fuchiwaki, Y., Yasuzawa, M., 2016. A fine pointed glucose oxidase immobilized electrode for low-invasive amperometric glucose monitoring. Biosens. Bioelectron. 86, 90–94. https://doi.org/10.1016/j.bios.2016.06.037.

López Marzo, A.M., Mayorga-Martinez, C.C., Pumera, M., 2020. 3D-printed graphene direct electron transfer enzyme biosensors. Biosens. Bioelectron. 151 https://doi.org/10.1016/j.bios.2019.111980.

Lopez, R.J., Babanova, S., Artyushkova, K., Atanassov, P., 2015. Surface modifications for enhanced enzyme immobilization and improved electron transfer of PQQ-dependent glucose dehydrogenase anodes. Bioelectrochemistry 105, 78–87. https://doi.org/10.1016/j.bioelechem.2015.05.010.

Marquitan, M., Mark, M.D., Ernst, A., Muhs, A., Herlitze, S., Ruff, A., Schuhmann, W., 2020. Glutamate detection at the cellular level by means of polymer/enzyme multilayer modified carbon nanoelectrodes. J. Mater. Chem. B 8, 3631–3639. https://doi.org/10.1039/c9tb02461a.

Milton, R.D., Wang, T., Knoche, K.L., Minteer, S.D., 2016. Tailoring biointerfaces for electrocatalysis. Langmuir 32, 2291–2301. https://doi.org/10.1021/acs.langmuir.5b04742.

Min, J., Sempionatto, J.R., Teymourian, H., Wang, J., Gao, W., 2021. Wearable electrochemical biosensors in North America. Biosens. Bioelectron. 172, 112750. https://doi.org/10.1016/j.bios.2020.112750.

Mohan, A.M.V., Windmiller, J.R., Mishra, R.K., Wang, J., 2017. Continuous minimally-invasive alcohol monitoring using microneedle sensor arrays. Biosens. Bioelectron. 91, 574–579. https://doi.org/10.1016/j.bios.2017.01.016.

Okuda-Shimazaki, J., Yoshida, H., Sode, K., 2020. FAD dependent glucose dehydrogenases – discovery and engineering of representative glucose sensing enzymes -. Bioelectrochemistry 132, 107414. https://doi.org/10.1016/j.bioelechem.2019.107414.

Palanisamy, S., Velusamy, V., Chen, S.W., Yang, T.C.K., Balu, S., Banks, C.E., 2019. Enhanced reversible redox activity of hemin on cellulose microfiber integrated reduced graphene oxide for H2O2 biosensor applications. Carbohydr. Polym. 204, 152–160. https://doi.org/10.1016/j.carbpol.2018.10.001.

Pettersen, E.F., Goddard, T.D., Huang, C.C., Couch, G.S., Greenblatt, D.M., Meng, E.C., Ferrin, T.E., 2004. UCSF Chimera - a visualization system for exploratory research and analysis. J. Comput. Chem. https://doi.org/10.1002/jcc.20084.

Ravenna, Y., Xia, L., Gun, J., Mikhaylov, A.A., Medvedev, A.G., Lev, O., Alfonta, L., 2015. Biocomposite based on reduced graphene oxide film modified with phenothiazone and flavin adenine dinucleotide-dependent glucose dehydrogenase for glucose sensing and biofuel cell applications. Anal. Chem. 87, 9567–9571. https://doi.org/10.1021/acs.analchem.5b02949.

Sasaki, K., Furusawa, H., Nagamine, K., Tokito, S., 2018. Charge-accumulative potentiometric measurements for ammonia detection using an enzymatic cascade reaction on a prussian blue electrode. Chem. Lett. 47, 1412–1415. https://doi.org/10.1246/cl.180692.

Schlesinger, O., Pasi, M., Dandela, R., Meijler, M.M., Alfonta, L., 2018. Electron transfer rate analysis of a site-specifically wired copper oxidase. Phys. Chem. Chem. Phys. 20, 6159–6166. https://doi.org/10.1039/c8cp00041g.

Sempionatto, J.R., Lin, M., Yin, L., De la paz, E., Pei, K., Sonsa-ard, T., de Loyola Silva, A. N., Khorshed, A.A., Zhang, F., Tostado, N., Xu, S., Wang, J., 2021. An epidermal patch for the simultaneous monitoring of haemodynamic and metabolic biomarkers. Nat. Biomed. Eng. https://doi.org/10.1038/s41551-021-00685-1.

Stergiou, A., Cantón-Vitoria, R., Psarrou, M.N., Economopoulos, S.P., Tagmatarchis, N., 2020. Functionalized graphene and targeted applications – highlighting the road from chemistry to applications. Prog. Mater. Sci. 114, 100683. https://doi.org/10.1016/j.pmatsci.2020.100683.

Strakosas, X., Selberg, J., Pansodtee, P., Yonas, N., Manapongpun, P., Teodorescu, M., Rolandi, M., 2019. A non-enzymatic glucose sensor enabled by bioelectronic pH control. Sci. Rep. 9, 1–7. https://doi.org/10.1038/s41598-019-46302-9.

Vilian, A.T.E., Kim, W., Park, B., Oh, S.Y., Kim, T.Y., Huh, Y.S., Hwangbo, C.K., Han, Y. K., 2019. Efficient electron-mediated electrochemical biosensor of gold wire for the rapid detection of C-reactive protein: a predictive strategy for heart failure. Biosens. Bioelectron. 142, 111549. https://doi.org/10.1016/j.bios.2019.111549.

Wang, A., Ding, Y., Li, L., Duan, D., Mei, Q., Zhuang, Q., Cui, S., He, X., 2019. A novel electrochemical enzyme biosensor for detection of 17β-estradiol by mediated electron-transfer system. Talanta 192, 478–485. https://doi.org/10.1016/j.talanta.2018.09.018.

Wang, S., Humphreys, E.S., Chung, S.Y., Delduco, D.F., Lustig, S.R., Wang, H., Parker, K. N., Rizzo, N.W., Subramoney, S., Chiang, Y.M., Jagota, A., 2003. Peptides with selective affinity for carbon nanotubes. Nat. Mater. 2, 196–200. https://doi.org/10.1038/nmat833.

Willner, I., Katz, E., 2000. Integration of layered redox proteins and conductive supports for bioelectronic applications. Angew. Chem. Int. Ed. Engl. https://doi.org/10.1002/(SICI)1521-3773(20000403)39:7.

Xia, L., Han, M., Zhou, L., Huang, A., Yang, Z., Wang, T., Li, F., Yu, L., Tian, C., Zang, Z., Yang, Q., Liu, C., Hong, W., Lu, Y., Alfonta, L., Wang, J., 2019. S-Click reaction for isotropic orientation of oxidases on electrodes to promote electron transfer at low potentials. Angew. Chem. 131, 16632–16636. https://doi.org/10.1002/ange.201909203.

Yao, H., Shum, A.J., Cowan, M., Lähdesmäki, I., Parviz, B.A., 2011. A contact lens with embedded sensor for monitoring tear glucose level. Biosens. Bioelectron. 26, 3290–3296. https://doi.org/10.1016/j.bios.2010.12.042.

Yuan, M., Minteer, S.D., 2019. Redox polymers in electrochemical systems: from methods of mediation to energy storage. Curr. Opin. Electrochem. 15, 1–6. https://doi.org/10.1016/j.coelec.2019.03.003.

Zhao, J., Lin, Y., Wu, J., Nyein, H.Y.Y., Bariya, M., Tai, L.C., Chao, M., Ji, W., Zhang, G., Fan, Z., Javey, A., 2019. A fully integrated and self-powered smartwatch for continuous sweat glucose monitoring. ACS Sens. 4, 1925–1933. https://doi.org/10.1021/acssensors.9b00891.

Zhou, F., Jing, W., Xu, Y., Chen, Z., Jiang, Z., Wei, Z., 2019. Performance enhancement of ZnO nanorod-based enzymatic glucose sensor via reduced graphene oxide deposition and UV irradiation. Sensor. Actuator. B Chem. 284, 377–385. https://doi.org/10.1016/j.snb.2018.12.141.